INTERNATIONAL JOURNAL OF HYDROGEN ENERGY XXX (2016) 1–9

Available online at www.sciencedirect.com

ScienceDirect

journal homepage: www.elsevier.com/locate/he

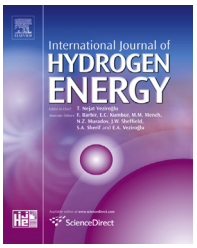

Cyclic stability and structure of nanoconfined Ti-doped $NaAlH_4$

Mark Paskevicius [a,*], *Uffe Filsø* [a], *Fahim Karimi* [b], *Julián Puszkiel* [b,c], *Philipp Klaus Pranzas* [b], *Claudio Pistidda* [b], *Armin Hoell* [d], *Edmund Welter* [e], *Andreas Schreyer* [b], *Thomas Klassen* [b], *Martin Dornheim* [b], *Torben R. Jensen* [a]

[a] *Interdisciplinary Nanoscience Center (iNANO) and Department of Chemistry, Aarhus University, Langelandsgade 140, DK-8000 Århus C, Denmark*

[b] *Institute of Materials Research, Materials Technology, Helmholtz-Zentrum Geesthacht, Max-Planck-Strasse 1, D-21502 Geesthacht, Germany*

[c] *Consejo Nacional de Investigaciones Científicas y Técnicas (CONICET) and Centro Atómico Bariloche, Av. Bustillo 9500, R8402AGP S. C. de Bariloche, Río Negro, Argentina*

[d] *Helmholtz-Zentrum Berlin für Materialien und Energie, Hahn-Meitner Platz 1, D-14109 Berlin, Germany*

[e] *HASYLAB at DESY, Notkestraße 85, D-22603 Hamburg, Germany*

ARTICLE INFO

Article history:
Received 15 June 2015
Received in revised form
23 October 2015
Accepted 25 December 2015
Available online xxx

Keywords:
Nanoconfinement
Hydrogen storage
In-situ
Structure

ABSTRACT

$NaAlH_4$ was melt infiltrated within a CO_2 activated carbon aerogel, which had been pre-loaded with $TiCl_3$. Nanoconfinement was verified by Small Angle X-Ray Scattering (SAXS) and the nature of the Ti was investigated with Anomalous SAXS (ASAXS) and X-Ray Absorption Near Edge Structure (XANES) to determine its size and chemical state. The Ti is found to be in a similar state to that found in the bulk Ti-doped $NaAlH_4$ system where it exists as $Al_{1-x}Ti_x$ nanoalloys. Crystalline phases exist within the carbon aerogel pores, which are analysed by *in-situ* Powder X-Ray Diffraction (PXD) during hydrogen cycling. The *in-situ* data reveals that the hydrogen release from $NaAlH_4$ and its hydrogen uptake occurs through the Na_3AlH_6 intermediate when confined at this size scale. The hydrogen capacity from the nanoconfined $NaAlH_4$ is found to initially be much higher in this CO_2 activated aerogel compared with previous studies into unactivated aerogels.

Introduction

Despite the extreme and exponentially increasing human energy consumption there is plenty of renewable energy available to us, but unfortunately these energy sources strongly fluctuate over time and geography. The most difficult challenge appears to be the development of efficient and reliable long-term energy storage, over days, weeks and months [1]. Hydrogen is an excellent energy storage medium, with the highest gravimetric energy storage density. The low volumetric energy storage density of hydrogen gas can be

* *Corresponding author.*
E-mail address: mark.paskevicius@gmail.com (M. Paskevicius).

http://dx.doi.org/10.1016/j.ijhydene.2015.12.185

greatly improved through its storage in a solid-state hydride. To date, $NaAlH_4$ is one of the most promising hydrogen storage compounds from a commercial stand point due to its low cost, moderate operating temperature and practical operating pressures. As such, ongoing research is focused on optimizing large scale $NaAlH_4$ tanks for energy storage applications [2,3]. It is well known that $NaAlH_4$ decomposes, releasing hydrogen in 3 steps:

$$3NaAlH_4 \leftrightarrows Na_3AlH_6 + 2Al + 3H_2 \quad ;3.70 \text{ wt.\%H} \tag{1}$$

$$Na_3AlH_6 \leftrightarrows 3NaH + Al + \tfrac{3}{2}H_2 \quad ;1.85 \text{ wt.\%H} \tag{2}$$

$$NaH \leftrightarrows Na + \tfrac{1}{2}H_2 \quad ;1.85 \text{ wt.\%H} \tag{3}$$

The first two steps release 5.6 wt.% H at moderate temperatures, whilst the third step is not usually utilised due to its high temperature requirements (~400 °C). Fast and low temperature hydrogen release and absorption was first realised in 1997 [4] through the addition of a $TiCl_3$ additive. This seminal research initiated a plethora of experimental and theoretical studies into the catalytic mechanism of low temperature hydrogen release and uptake in $NaAlH_4$. The mechanism was only recently determined through a series of detailed and focussed experimental studies into doped $NaAlH_4$ [5–11]. The $TiCl_3$ is reduced by $NaAlH_4$, forming NaCl, Al, and a selection of $Al_{1-x}Ti_x$ nanoalloys on the surface of the $NaAlH_4$ crystallites [5]. These Al–Ti nanoparticles provide dissociation sites for H_2 gas, increasing the kinetics of hydrogen absorption into decomposed $NaAlH_4$ [9]. The same Al–Ti nanoparticles can also influence the Al–H bonding to enable low temperature hydrogen release [9]. This bifunctional mechanism is the key to fast absorption and desorption kinetics in the $NaAlH_4$ system. The functionality of the Al–Ti nanoparticles is highly dependent on the morphology of the sample, where the Al–Ti must be in close contact with the $NaAlH_4$ whilst being accessible to H_2 gas [9]. This intimate contact may be manufactured and maintained through the process of nanoconfinement.

Nanoconfinement involves the incorporation of a compound within a porous framework. The framework controls the particle size of an incorporated compound by its pore size and also restricts long-range phase segregation during hydrogen release and uptake [12,13]. The importance of the CO_2 activation process in carbon aerogel synthesis was recently highlighted in regard to its advantages for nanoconfinement [14]. The CO_2 activation process reduced oxygen impurities from the scaffold whilst increasing the surface area. This means that the aerogel scaffold is less reactive towards oxygen-sensitive materials, allowing improved hydrogen capacity and better reversibility of nanoconfined hydrides. The reduction of functional groups from carbon aerogel during heat treatment and CO_2 activation is well known [15]. However, depending on synthesis conditions, some functional groups can still remain in the carbon aerogel after heat treatment to 1050 °C [16]. The cyclic stability of nanoconfined hydrides is not only related to the inertness of the scaffold. Significant levels of degradation in nanoconfined $NaAlH_4$ were recently observed [17] due to expulsion of reaction products from the scaffold under vacuum at high temperatures. However, this study relates to nanoconfinement within an ordered mesoporous carbon, and the effect of pore ordering on confinement permanency is not yet known.

The investigation into nanoconfined $TiCl_3$ doped $NaAlH_4$ was recently conducted [18], demonstrating that it provided faster rates of hydrogen evolution than undoped nanoconfined $NaAlH_4$. However, in this study the carbon aerogel was not CO_2 activated during synthesis, leading to a low aerogel surface area (735 m^2/g) and a high likelihood of reactive functional groups in the scaffold. In fact, there is a significant proportion of Al present after $NaAlH_4$ infiltration, indicating a reaction with the scaffold. This is further supported by the low hydrogen capacity achievable, only 2.9 wt.% H instead of the expected >5 wt.% H.

In the current study we aim to infiltrate $TiCl_3$ doped $NaAlH_4$ into a CO_2 activated carbon aerogel, limiting the degree of scaffold reactivity. We aim to investigate the cyclic stability of nanoconfined Ti-doped $NaAlH_4$ and also determine information about the state of the Ti-based additive in the nanoconfined system.

Material and methods

Aerogel synthesis

Carbon aerogel (CA) was synthesized according to a well-known method [19] from a resorcinol-formaldehyde pathway using a sodium carbonate catalyst. The reagents, resorcinol (41.791 g), formaldehyde (56.9 mL), and Na_2CO_3 (0.034 g) were stirred in water (56.6 mL) for 2 h. The mixture was then aged at room temperature for 24 h, 50 °C for 24 h, and then 90 °C for 72 h. The gels were then washed with acetone 3 times and dried in air overnight at room temperature. Next, the gels were pyrolysed under flowing nitrogen (50 mL/min) by heating from room temperature to 840 °C at 2.6 °C/min, holding for 6 h, and then cooling back to room temperature at 15 °C/min.

Activation of the aerogels was performed using CO_2 treatment to increase the total pore volume and surface area [15]. The aerogels were activated under flowing CO_2 (50 mL/min) during heating from room temperature to 920 or 940 °C, holding for 5.5 h, and then cooling back to room temperature at 15 °C/min.

Three different aerogels were synthesized as shown in Table 1.

After synthesis, all aerogels were degassed by heating to 400 °C under dynamic vacuum for several hours to remove traces of air and moisture from the porous framework. The degassed aerogels were then transferred into an argon

Table 1 – CO_2 activation parameters for as-synthesised samples.

Name	CO_2 activated	Activation temperature (°C)	Material loss (%)
X	No	–	–
XA1	Yes	920	39.9
XA2	Yes	940	45.6

Please cite this article in press as: Paskevicius M, et al., Cyclic stability and structure of nanoconfined Ti-doped $NaAlH_4$, International Journal of Hydrogen Energy (2016), http://dx.doi.org/10.1016/j.ijhydene.2015.12.185

glovebox without air exposure. All further sample handling was performed under argon.

$TiCl_3$ infiltration

Each aerogel sample was infiltrated with $TiCl_3$ as a hydrogen uptake/release catalyst for $NaAlH_4$. A quantitative solution of $TiCl_3$ in acetone was prepared under argon and added to each aerogel followed by stirring for 2 h at 30 °C. The acetone was then removed via evacuation into a Schleck line at room temperature for 2 h followed by 16 h at 190 °C. The mass of each sample was measured before and after $TiCl_3$ infiltration to determine the loading, as shown in Table 2.

$NaAlH_4$ melt infiltration

$NaAlH_4$ was infiltrated into the $TiCl_3$-doped carbon aerogels using a known melt infiltration technique [18]. Mixtures of the $NaAlH_4$ and CA were loaded into a high pressure autoclave under ~200 bar of hydrogen. The autoclave was then heated from room temperature to 189 °C at 2 °C/min before holding for 15 min and then cooling back to room temperature. The aerogels were loaded with 40–50 wt.% $NaAlH_4$ as shown in Table 2. It should be noted that a high hydrogen pressure was used during melt infiltration to prevent decomposition of the $NaAlH_4$. At 189 °C the equilibrium pressure for $NaAlH_4$ is 143 bar, based on its thermodynamics [20].

A sample was also prepared by ballmilling XA1-Ti with 75.1 wt.% $NaAlH_4$ on a Fritsch Pulverisette 4 using WC vials and balls for 30 min at 250 rpm with 2 min on/off cycles.

Characterization

Nitrogen sorption was performed on a Nova 2200e surface area and pore size analyser from Quantachrome Instruments. The surface area was calculated using the Brunauer–Emmett–Teller (BET) method. Hydrogen-based Sieverts measurements were performed on a PCTPro-2000 (Setaram). Hydrogen cycled samples were cycled twice. Desorption cycles were conducted in an evacuated volume by performing a 2 °C/min ramp to 100 °C, holding for 4 h, followed by a 2 °C/min ramp to 220 °C, holding for 10 h. Absorption cycles were performed under 100 bar H_2 during a thermal ramp from room temperature to 160 °C at 1 °C/min, holding for 10 h.

Laboratory powder X-ray diffraction (PXD) data were collected with a Rigaku diffractometer using Cu Kα radiation, corresponding to a wavelength of 1.544 Å. Synchrotron *in-situ* powder X-ray diffraction (SR-PXD) experiments were conducted at I711 beamline at MAXLab, Sweden using a wavelength of 1.009816 Å and 30 s exposure times. Samples for *in-situ* studies were packed in 0.79 mm inner diameter sapphire tubes (Al_2O_3) and were heated at a controlled rate using a Ni–Cr element heater on custom apparatus [21].

Small angle X-ray scattering (SAXS) was performed on the high brilliance SAS/USAXS beamline BW4 in Hasylab at the Deutsches Elektronen-Synchrotron (DESY), Hamburg, Germany. The beamline was equipped with a MAR CCD detector and the measurements were carried out at two distances (1.8 m and 8 m), respectively, so that the maximum accessible range of scattering vector is covered, where $q = (4\pi/\lambda)\sin\theta$, λ and 2θ being the incident wavelength of the photons and the scattering angle of the photons, respectively. The applied wavelength was set to 1.38 Å (8.98 keV). All samples were sealed between Kapton tape in a sample holder with a circular window of 10 mm. The exposure time of the samples was set to 180 s, which gave good signal to noise ratios for all samples.

Anomalous Small angle X-ray scattering (ASAXS) was performed on the 7T-MPW-SAXS beamline in BESSY at the Helmholtz-Zentrum Berlin (HZB), Germany [22]. The beamline was equipped with a multi-wire proportional counter gas detector and the beamline has with an energy resolution of $\Delta E/E \sim 2 \times 10^{-4}$. In order to separate the resonant scattering of Ti-containing nanostructures, all measurements were carried out at four energies (4600 eV, 4905 eV, 4955 eV, 4964 eV) near but below the K absorption-edge of titanium. Furthermore, all measurements were performed at two sample-to-detector distances (0.7 m and 3.345 m) to cover the maximum possible experimental q-range. All samples were sealed between Kapton tape in a sample holder of thin molybdenum sheet with a circular window of 3 mm. Separation of the so called resonant scattering curves were achieved by using the separation method developed by Stuhrmann [23–25].

X-ray absorption near edge structure (XANES) was performed on the A1 beamline in Hasylab at the DESY. The samples were mixed with boron nitride and pressed into pellets of 10 mm in diameter. The pellets were enclosed between Kapton tape. The measurements were collected in transmission mode around the K absorption edge of titanium (4.9664 keV). The step width was chosen to be 2 eV and for each sample three XANES-spectra were recorded and their average was used. All references for titanium in different oxidation states were measured immediately after the samples on the same setup.

It should be mentioned that SAXS, ASAXS and XANES results refer to samples prepared from unactivated (lower surface area) aerogels, whereas PXD and hydrogen measurements were performed on activated aerogel samples. The prime difference between activated and unactivated aerogels is the surface area and pore size.

Table 2 – $TiCl_3$ and $NaAlH_4$ infiltration details for each aerogel.

Scaffold	$TiCl_3$ infiltration		$NaAlH_4$ infiltration	
Name	Name	$TiCl_3$ loading (wt.%)	Name	$NaAlH_4$ loading (wt.%)
X	X–Ti	7.4	X-Ti-Na	39.9
XA1	XA1-Ti	8.4	XA1-Ti-Na	49.9
XA2	XA2-Ti	8.0	XA2-Ti-Na	50.1

Results and discussion

Nature of nanoconfined Ti-doped $NaAlH_4$

Nitrogen sorption was performed on the as-synthesized carbon aerogels before infiltration as shown in Table 3. The aerogel that was not activated with CO_2 (X) had a surface area of

Please cite this article in press as: Paskevicius M, et al., Cyclic stability and structure of nanoconfined Ti-doped $NaAlH_4$, International Journal of Hydrogen Energy (2016), http://dx.doi.org/10.1016/j.ijhydene.2015.12.185

Table 3 – Nitrogen sorption results from as-synthesised carbon aerogels.

Aerogel	Surface area (±12 m^2/g)	Micropore volume (±0.02 mL/g)	Total pore volume (±0.02 mL/g)
X	910	0.28	1.21
XA1	1670	0.51	1.84
XA2	1830	0.55	2.03

912 m^2/g, larger than expected based on the synthesis method (700 m^2/g [26]). However, the total pore volume is 1.21 mL/g, somewhat lower than the volume observed previously, 1.3 mL/g. After CO_2 activation the surface area is dramatically increased (XA1 and XA2) as expected, providing a greater pore volume for infiltration.

PXD was performed on the carbon aerogels after the infiltration of $TiCl_3$ and $NaAlH_4$ to assess the crystallinity of the infiltrated compounds, as shown in Fig. 1. Directly after infiltration the PXD identifies crystalline $NaAlH_4$, Al, and $TiCl_3$. The presence of crystalline compounds after nanoconfinement matches previous work with similar aerogels [26]. However, other studies have shown the quenching of all X-ray diffraction peaks from $NaAlH_4$ after nanoconfinement in 10 nm pores of ordered mesoporous silica [27]. The presence of $TiCl_3$ in PXD indicates that it is not completely reduced by $NaAlH_4$ during infiltration. However, it is no longer present after hydrogen cycling. The presence of Al after infiltration indicates the decomposition of $NaAlH_4$, but without crystalline NaH or Na_3AlH_6 being present it is likely that some Na has been lost due to reactivity with the scaffold, forming unwanted amorphous by-products. This is also the case in other studies [18], where large quantities of crystalline Al are present after infiltration. Interestingly, no NaCl is detectable in the PXD after hydrogen cycling, even though the $TiCl_3$ is no longer present. It is likely that the NaCl is highly nanoscopic, which would result in very broad diffraction peaks that are difficult to detect.

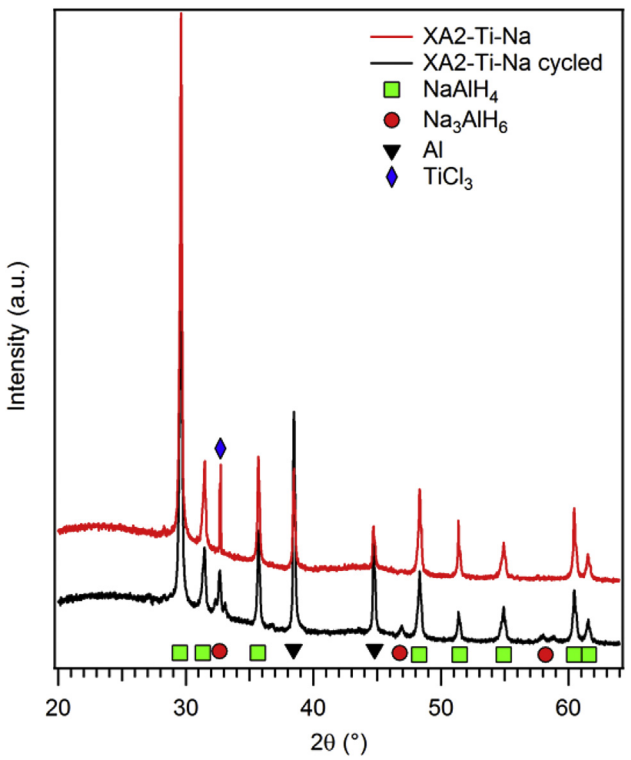

Fig. 1 – XRD data for XA2-Ti-Na and XA2-Ti-Na hydrogen cycled once, λ = 1.544 Å.

An important question regarding nanoconfinement is whether the compound is actually nanoconfined within the pore network, or simply on the surface of the framework. Detecting whether a compound is nanoconfined within the small pores of a framework is very difficult using electron microscopy. Transmission electron microscopy (TEM) can be used to image the pore network and energy dispersive spectroscopy (EDS) can be used to determine the presence of an infiltrated compound. However, it is hard to prove that the compound is in the pores, rather than on the surface of the framework. A recent study into $LiBH_4$–$Ca(BH_4)_2$ composites in porous carbon [28] was able to definitively prove that the compound was infiltrated, primarily because the scaffold was an ordered mesoporous carbon. Performing EDS in a step-wise fashion across the ordered pores and framework demonstrated Ca-rich areas within the pores. This technique is not possible with carbon aerogel because of its fractal-like pore network. However, small angle X-ray scattering (SAXS) is a very useful technique for detecting whether a porous scaffold has been infiltrated by another material [17,29]. Changes in the electron density within the pores are detected by SAXS, providing direct proof of nano-infiltration.

SAXS was performed on infiltrated carbon aerogels at an X-ray energy of 8.98 keV to investigate $NaAlH_4$ loading, as shown in Fig. 2. A pronounced Guinier shoulder is visible at 2 nm^{-1} for X–Ti prior to $NaAlH_4$ infiltration. The Guinier region occurs because of the electron density difference between the pores (mostly empty) and the carbon scaffold. SAXS data were fit using the unified model [30,31] due to its versatility in fitting a range of different structural features simultaneously. The unified model combines models of Guinier and power law features, which can provide structural information about CA pore sizes and surfaces (see Table 4). The unified fitting results for X–Ti show the presence of 2.8 nm pores (assuming they are spherical), which have slightly rough surfaces. Surface roughness is given by the high-q power law slope, where a slope of 3 indicates an incredibly rough surface and 4 indicates a smooth surface [32]. Upon $NaAlH_4$ infiltration the Guinier region is quenched (less prominent). This result is proof that $NaAlH_4$ infiltration is successful, because it indicates a change in the electron density within the pores [29]. The presence of $NaAlH_4$ creates a smaller electron density difference between the pores and the scaffold, lowering the scattering contrast. For empty pores the scattering contrast $(\Delta\rho)^2$ for CA is 2.88×10^{22} cm^{-4} but if the pores are fully loaded with $NaAlH_4$ then the scattering contrast drops to 0.37×10^{22} cm^{-4}. This means that upon loading the scattering from the pores can be reduced ~10-fold, which is seen by the reduction in the intensity of the Guinier in Fig. 2.

The unified fit provides larger pore sizes after $NaAlH_4$ infiltration (4.3 nm instead of 2.8 nm). This can be explained by the presence of a pore size distribution in the sample. If the

Please cite this article in press as: Paskevicius M, et al., Cyclic stability and structure of nanoconfined Ti-doped $NaAlH_4$, International Journal of Hydrogen Energy (2016), http://dx.doi.org/10.1016/j.ijhydene.2015.12.185

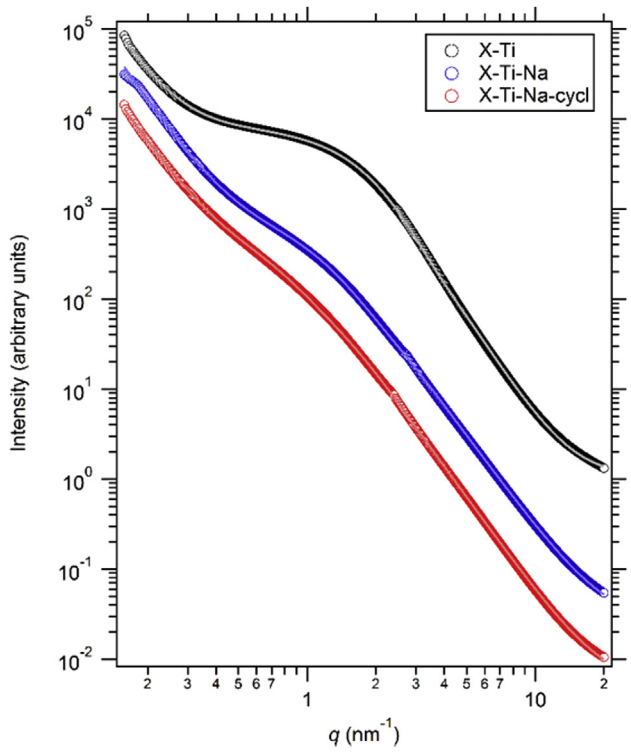

Fig. 2 – SAXS data for X–Ti, X-Ti-Na, and X-Ti-Na-cycled. Fitted curves are shown as solid lines.

smaller pores are filled more easily, then their scattering contrast is diminished. This would lead to a bias in the scattering observed from larger unfilled pores. This effect is more pronounced after cycling (6.4 nm), but is an indication that the $NaAlH_4$ and its decomposition products are still nanoconfined. This sample experienced low pressure during desorption, but was not under active vacuum. Previous studies have demonstrated that $NaAlH_4$ reaction products can be removed from the pores during hydrogen desorption under active vacuum [17].

There is a discrepancy between the $NaAlH_4$ average crystallite size from PXD (48 nm) and the average pore size from SAXS (2.8–6.4 nm). The SAXS results do give direct proof of $NaAlH_4$ infiltration into the carbon aerogel pores, however PXD indicated that much larger $NaAlH_4$ particles are also present in the sample. There are two main possibilities: 1) The $NaAlH_4$ is only partially infiltrated, with some $NaAlH_4$ in pores and some on the surface of the carbon aerogel, or 2) The carbon aerogel also has larger pores that are filled with bigger $NaAlH_4$ particles, which are detectable by XRD, but on the limit of the SAXS studies.

Anomalous small angle X-ray scattering (ASAXS) was utilized to investigate the structure of the titanium-bearing compounds in the as-infiltrated sample, after $NaAlH_4$ loading and after hydrogen cycling, as shown in Fig. 3. Each resonant scattering pattern displays a characteristic Guinier shoulder, demonstrating that Ti is present in the form of small particles in all samples. The unified model was also used to fit the ASAXS data, where fitting results are provided in Table 4. The Ti compounds are present as 2.4 nm particles in the $TiCl_3$ loaded CA, close to the average pore size of the aerogel after $TiCl_3$ loading (2.8 nm). This means that, on average, the $TiCl_3$ tends to mostly fill certain pores within the CA (average particle size is close to average pore size). The particle size of the Ti-compound(s) does not greatly change upon $NaAlH_4$ addition or thermal cycling. Therefore, even when $TiCl_3$ reacts with $NaAlH_4$, as is thermodynamically favourable, its particle size does not greatly change. This is likely due to the fact that it is nanoconfined and unable to grow further, which is contrary to unconfined systems [33–37]. However, the surface of the Ti compounds does change after $NaAlH_4$ addition and after thermal cycling. The high-q power law slope approaches 3, indicating rougher surfaces on the Ti-bearing particles.

Further information can be gained about the nature of the Ti in the nanoconfined sample by performing X-ray absorption near edge structure (XANES) measurements to probe the chemical bonding information from Ti. Fig. 4 displays the Ti absorption edge for nanoconfined samples and a range of

Table 4 – SAXS and ASAXS-Ti unified fit details for each aerogel.

		X–Ti	X-Ti-Na	X-Ti-Na-cycled
SAXS	Low-q power law slope	3.7	3.5	3.5
	Radius of gyration (nm)	1.1	1.7	2.5
	Diameter (nm)	2.8	4.3	6.4
	High-q power law slope	3.8	3.4	3.5
ASAXS-Ti	Radius of gyration (nm)	0.9	1.0	1.1
	Diameter (nm)	2.4	2.6	2.9
	High-q power law slope	4.0	3.6	3.4

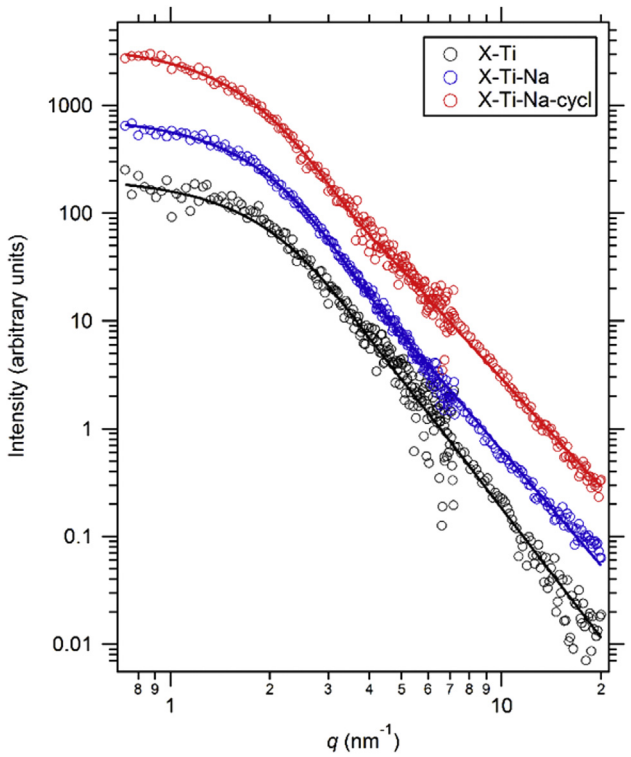

Fig. 3 – ASAXS results (Ti K edge) of samples X–Ti, X-Ti-Na, and X-Ti-Na-cycl. The extracted resonant scattering curves are shown. Fitted curves are shown as solid lines.

Please cite this article in press as: Paskevicius M, et al., Cyclic stability and structure of nanoconfined Ti-doped $NaAlH_4$, International Journal of Hydrogen Energy (2016), http://dx.doi.org/10.1016/j.ijhydene.2015.12.185

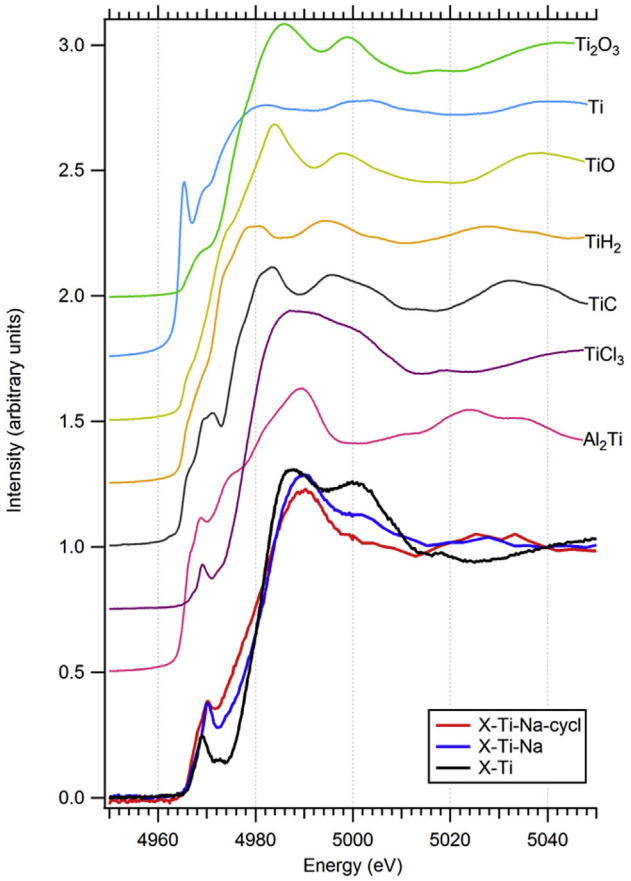

Fig. 4 – XANES measurements of samples X–Ti, X-Ti-Na, and X-Ti-Na-cycl. and reference materials.

standard Ti-containing materials. XANES has previously been applied to the bulk Ti-doped $NaAlH_4$ system [38]. These results indicated that the Ti valence was zero, without change after hydrogen cycling. In this case, qualitative comparisons of the Ti edge structure suggested that Ti was present in the form of amorphous Al_3Ti. Since this study was performed we now know that the Ti is most likely in the form of $Al_{1-x}Ti_x$ amorphous alloy nanoparticles [5], which also correlates well with the XANES data for the bulk system.

The XANES results for the nanoconfined system are provided in Fig. 4. The $NaAlH_4$ infiltrated sample has a very similar Ti edge structure before and after hydrogen cycling, indicating that the Ti containing phase(s) does not significantly change over 2 cycles. The $NaAlH_4$ infiltrated samples do differ from the aerogel that has only been $TiCl_3$ loaded (X–Ti). After the initial $TiCl_3$ loading the Ti edge resembles that of the pure $TiCl_3$ standard, but there is a more pronounced peak at 5000 eV, which also appears in the Ti_2O_3 standard. This could indicate a minor reaction between the chloride and oxygen in the carbon aerogel scaffold as it is possible that the scaffold still contains minor oxygen impurities. The 5000 eV feature is less pronounced in the $NaAlH_4$ infiltrated sample (X-Ti-Na) and absent after hydrogen cycling. This may indicate the reduction of the oxide by $NaAlH_4$. The strong peak at 4990 eV in the $NaAlH_4$ loaded samples matches closely with the Al_2Ti standard, however the lower edge structure appears more similar to the $TiCl_3$ standard. It is possible that some of the $TiCl_3$ is still present in the scaffold in a nanocrystalline state, isolated from $NaAlH_4$ and unable to react. This would mean that Ti is present in multiple valences in different compounds, making the XANES analysis more complicated due to a convolution of Ti edge structures. However, these results do indicate that the reacted Ti is in the form of an Al–Ti alloy, in line with what is observed in the bulk system. This means that the same catalytic mechanism for hydrogen absorption and release can be expected, but the nanoconfinement restricts the $NaAlH_4$ particle size and hence limits phase segregation of reaction products upon cycling.

Hydrogen cycling behaviour

Hydrogen desorption and absorption cycles were performed (Fig. 5) on the nanoconfined Ti-doped $NaAlH_4$ (XA2-Ti-Na)

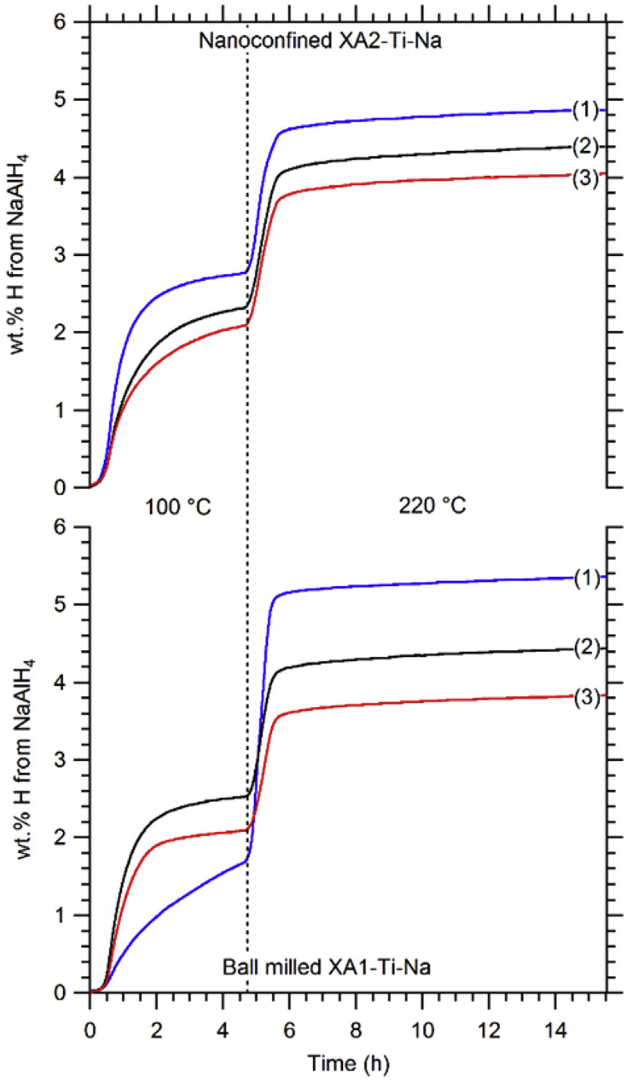

Fig. 5 – Hydrogen release from nanoconfined and ballmilled samples. The wt.% H is relative to the $NaAlH_4$ content in the samples. Reabsorption was performed at 160 °C under 140 bar H_2. Hydrogen release profiles are provided for the first 3 desorption cycles.

Please cite this article in press as: Paskevicius M, et al., Cyclic stability and structure of nanoconfined Ti-doped $NaAlH_4$, International Journal of Hydrogen Energy (2016), http://dx.doi.org/10.1016/j.ijhydene.2015.12.185

along with a reference sample, where XA1-Ti was ball milled with 75 wt.% $NaAlH_4$. The reference sample was assessed to compare the hydrogen kinetics and cycling capacity between a nanoconfined sample and an intimate mixture of the compounds. Hydrogen desorption was studied during two temperature steps at 100 °C and 220 °C, where a maximum hydrogen capacity of ~5.5 wt.% H was expected, with no decomposition expected from NaH. However, it is possible that NaH could desorb hydrogen at these low temperatures as previous research has shown vastly increased desorption kinetics from NaH in intimate contact with nanoporous carbon [39]. Desorption was undertaken by releasing gas into an evacuated volume, whereas absorption was performed under 140 bar of H_2 at 160 °C for 10 h.

As shown in Fig. 5, the nanoconfined sample displays rapid desorption kinetics and reaches 90% of the expected maximum capacity (4.8 wt.% H) in the first cycle. A slight degradation in kinetics can be observed in further cycles at 100 °C by reductions in the slope of the hydrogen release profile. In addition, further drops in the maximum capacity are also observed, where only 4 wt.% H is released on the third cycle. The drop in capacity is not as large as previously observed [18], possibly due to the reduced oxygen content in the CO_2 activated aerogels used in the present study. The observed maximum capacity herein is also much closer to the theoretical maximum, 90% instead of ~50% in this previous study [18]. The capacity loss observed during cycling could be due to reactions between the $NaAlH_4$ and the scaffold or could be due to nanoconfinement degradation. A recent study demonstrated that $NaAlH_4$ or its byproducts can be extracted from the scaffold during high temperature decomposition [17]. The melting point of $NaAlH_4$ is 182 °C [40] and if low external pressures or high internal pressures within the scaffold are experienced, then the $NaAlH_4$ could be extracted in the molten phase before decomposition has begun. The extraction of $NaAlH_4$ from the scaffold could reduce its contact with catalytic Al–Ti particles and it may also result in phase segregation.

The kinetic behaviour of hydrogen release from the ball milled sample at 100 °C are initially much slower than those for the nanoconfined sample (blue curves (in the web version) in Fig. 5). The ball milling treatment should have intimately mixed the $NaAlH_4$ and $TiCl_3$, resulting in a reduction reaction and the formation of NaCl and Al–Ti nanoparticles. The presence of carbon and minor levels of oxygen are not usually present in the preparation of bulk samples of $NaAlH_4$ and they may influence the surface morphology of the $NaAlH_4$ particles, which has been shown to be vital to the hydrogen kinetics [9]. A more pronounced degradation in the maximum hydrogen capacity is observed in the ball milled sample compared to the nanoconfined sample (1.6 wt.% H instead of 0.8 wt.% H). This is somewhat unexpected as the cyclic capacity of bulk Ti-doped $NaAlH_4$ is very stable [41]. Although, poor cyclability has also been previously observed in samples ball milled with carbon aerogel [18]. Poor cyclability indicates either phase segregation (kinetically limiting further reactions) or adverse reactions between the $NaAlH_4$ and the scaffold (consuming reaction products). Nanoconfinement should restrict phase segregation, thus making the reactivity between $NaAlH_4$ and the scaffold most likely. However, the presence of carbon can be beneficial to hydrogenation and dehydrogenation from $NaAlH_4$. A study into bulk mixtures of $NaAlH_4$ with turbostratic carbon (planar structure) indicated the presence of Na intercalation of the carbon, which could aid hydrogenation reactions with altered thermodynamics [39].

In order to better understand how the system behaves during hydrogen cycling, *in-situ* SR-PXD data were collected during desorption and adsorption cycles of nanoconfined Ti-doped $NaAlH_4$ (XA1-Ti-Na). The sample was heated from room temperature to 110 °C and kept at a fixed temperature throughout hydrogen cycling. The pressure was cycled between 140 bar and vacuum every 15 min after the desired temperature was reached. There is a very noticeable increase in the scattering background at ~16.5° 2θ, at $d = 3.5$ Å when hydrogen pressure is applied. The hump in the background (dark region in Fig. 6) then disappears upon evacuation of the system. The *d*-spacing of this hump matches that of the (0 0 2) reflection of amorphous carbon [42], but it is unclear as to why this feature would become so prominent under high gas pressure. This hump in the scattering background is also centred about the (0 1 2) position for Al_2O_3 (sapphire) at $d = 3.48$ Å. It is possible that the gas pressure introduces an amorphous section of the sapphire capillary into the X-ray beam, generating a large hump in the background.

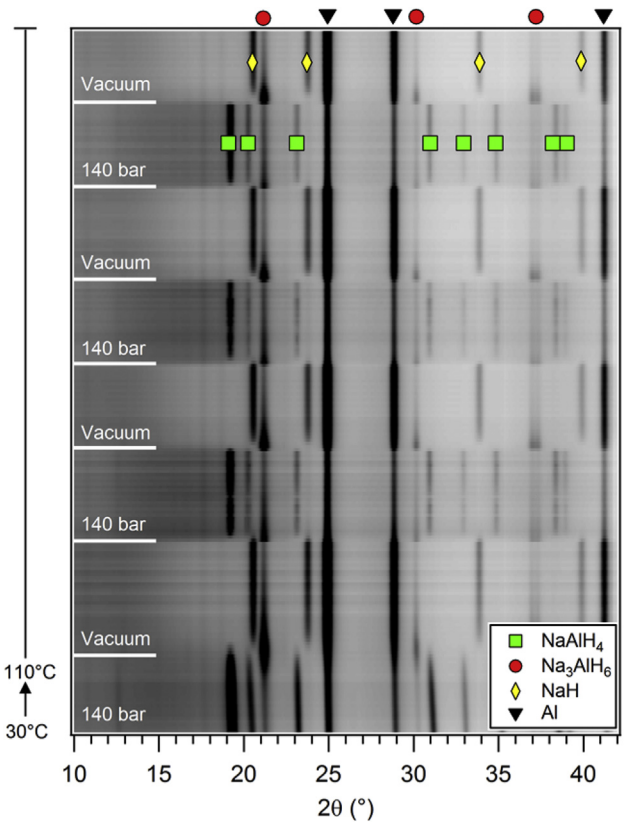

Fig. 6 – In situ SR-PXD data, λ = 1.0098 Å, showing desorption and absorption cycles of melt infiltrated $NaAlH_4$ in activated aerogel (XA1-Ti-Na). The hydrogen pressure is cycled between 140 bar and vacuum multiple times after the sample is heated from room temperature to 110 °C.

Please cite this article in press as: Paskevicius M, et al., Cyclic stability and structure of nanoconfined Ti-doped $NaAlH_4$, International Journal of Hydrogen Energy (2016), http://dx.doi.org/10.1016/j.ijhydene.2015.12.185

Initially the sample is predominantly $NaAlH_4$ with some Na_3AlH_6 and Al. No NaH can be observed nor can NaCl, the expected reaction byproduct from $TiCl_3$ doping. However, there is a strong overlap between the diffraction peaks of NaCl and the other phases present, so NaCl would be difficult to discern from this medium resolution diffraction data. Interestingly we also observe that initially there is unreacted Na_3AlH_6 and Al, which does not react even under 140 bar at 100 °C. This phenomena is well known in the bulk Ti-doped $NaAlH_4$ system [43] where $Al_{1-x}Ti_x$ phases can trap Al and prevent it from reacting with Na_3AlH_6. In the bulk system, excess Al can be added to provide enough Al for the reaction to go to completion, eliminating dead-weight Na_3AlH_6 and allowing for the complete rehydrogenation of $NaAlH_4$. The addition of excess Al within a nanoconfined system is not currently feasible.

Upon evacuation, the $NaAlH_4$ diffraction peaks disappear and a rapid transition through the Na_3AlH_6 intermediate is observed, followed by the formation of NaH and more Al. Rehydrogenation under 140 bar also proceeds through the Na_3AlH_6 intermediate. The second hydrogen absorption cycle regenerates $NaAlH_4$, but the diffraction peaks are less intense than before cycling began. This is an indication of hydrogen capacity loss in the system, which is less noticeable in further cycles.

Some studies into the nanoconfinement of $NaAlH_4$ have reported changes in the thermodynamics of the decomposition reaction pathway [44,45] from pressure-composition studies. The results indicate that the Na_3AlH_6 compound is not formed under its normally observed pressure and temperature conditions. However, we still observe Na_3AlH_6 as an intermediate product in our *in-situ* study. It is likely that the thermodynamic changes are only observed for nanoconfinement in very small pores when long range crystalline order is no longer possible and X-ray diffraction can no longer detect the nanoconfined products.

Conclusions

Nanoconfinement has been a promising technique to enhance the properties of hydrogen storage materials for almost a decade. Although many studies have been performed on $NaAlH_4$, the mechanism of kinetic enhancement during nanoconfinement is still barely understood. This study has aimed to investigate the cyclic stability of nanoconfined Ti-doped $NaAlH_4$ and also determine information about the state of the Ti-based additive in the nanoconfined system. The hydrogen capacity from nanoconfined $NaAlH_4$ is found to be much higher in this CO_2 activated aerogel compared with previous studies into unactivated aerogels. The presence of high levels of residual O-containing surface groups in unactivated aerogels is likely detrimental towards reactive $NaAlH_4$ and a major factor in reducing the hydrogen capacity of nanoconfined hydrides. However, there is polydispersity in the $NaAlH_4$ particle size, given by differences between PXD and SAXS results. This polydispersity could mean that the $NaAlH_4$ infiltration was only partial, or that it is spread across a large range of pore sizes. Larger $NaAlH_4$ particles will act like bulk NaAlH4, also causing bulk-like hydrogen desorption properties.

The combination of analytical techniques has shown a number of new insights into the behaviour and structural nature of this system. Of particular importance in understanding catalysed $NaAlH_4$, the Ti is found to be in a similar state to that found in the bulk Ti-doped $NaAlH_4$ system where it exists as $Al_{1-x}Ti_x$ nanoalloys. These alloys do not greatly change structure during hydrogen cycling, maintaining a consistent particle size. Nanoconfinement is confirmed and tracked using SAXS showing that the $NaAlH_4$ remains confined during hydrogen cycling. The positive results found using SAXS and ASAXS demonstrate that these techniques are vital tools in probing nanoconfined systems.

Acknowledgements

Beamline I711, MAXII laboratories, Lund, Sweden are thanked for the allocated beam time. Parts of this research were performed at the light source DORIS III at DESY, a member of the Helmholtz Association (HGF). The authors would like also to thank CONICET (Consejo Nacional de Invetigaciones Científicas y Tecnicas), and DAAD (German Academic Exchange Service) e Ministerio de Educación de la Nación Argentina (Sandwich Grant Program) (Grant Number – A/09/75212) for financial support to carry out this work. The authors acknowledge financial support from The Danish Council for Strategic Research via the research project *HyFillFast* and The Danish Council for Independent Research for DFF Mobility 1325-00072.

REFERENCES

[1] MacKay DJC. Sustainable energy – without the hot air. Cambridge: UIT; 2009.
[2] Bellosta von Colbe JM, Metz O, Lozano GA, Pranzas PK, Schmitz HW, Beckmann F, et al. Behavior of scaled-up sodium alanate hydrogen storage tanks during sorption. Int J Hydrogen Energy 2012;37:2807–11.
[3] Bellosta von Colbe JM, Lozano G, Metz O, Bücherl T, Bormann R, Klassen T, et al. Design, sorption behaviour and energy management in a sodium alanate-based lightweight hydrogen storage tank. Int J Hydrogen Energy 2015;40:2984–8.
[4] Bogdanović B, Schwickardi M. Ti-doped alkali metal aluminium hydrides as potential novel reversible hydrogen storage materials. J Alloys Compd 1997;253–254:1–9.
[5] Pitt MP, Vullum PE, Sørby MH, Blanchard D, Sulic M, Emerich H, et al. The location of Ti containing phases after the completion of the $NaAlH_4$ + $xTiCl_3$ milling process. J Alloys Compd 2012;513:597–605.
[6] Pitt MP, Vullum PE, Sørby MH, Sulic MP, Emerich H, Paskevicius M, et al. Functionality of the nanoscopic crystalline Al/amorphous $Al_{50}Ti_{50}$ surface embedded composite observed in the $NaAlH_4$ + $xTiCl_3$ system after milling. J Alloys Compd 2012;514:163–9.
[7] Pitt MP, Vullum PE, Sørby MH, Emerich H, Paskevicius M, Buckley CE, et al. Amorphous Al1–xTix, Al1–xVx, and Al1–xFex phases in the hydrogen cycled $TiCl_3$, VCl_3 and $FeCl_3$ enhanced NaAlH4 systems. J Alloys Compd 2012;521:112–20.
[8] Pitt MP, Vullum PE, Sørby MH, Emerich H, Paskevicius M, Buckley CE, et al. A structural review of nanoscopic $Al_{1-x}TM_x$ phase formation in the $TMCl_n$ enhanced $NaAlH_4$ system. J Alloys Compd 2012;527:16–24.

Please cite this article in press as: Paskevicius M, et al., Cyclic stability and structure of nanoconfined Ti-doped $NaAlH_4$, International Journal of Hydrogen Energy (2016), http://dx.doi.org/10.1016/j.ijhydene.2015.12.185

[9] Pitt MP, Vullum PE, Sørby MH, Emerich H, Paskevicius M, Buckley CE, et al. Hydrogen absorption kinetics of the transition-metal-chloride-enhanced $NaAlH_4$ system. J Phys Chem C 2012;116:14205–17.
[10] Pitt MP, Vullum PE, Sørby MH, Emerich H, Paskevicius M, Webb CJ, et al. Hydrogen absorption kinetics and structural features of $NaAlH_4$ enhanced with transition-metal and Ti-based nanoparticles. Int J Hydrogen Energy 2012;37:15175–86.
[11] Pitt MP, Vullum PE, Sørby MH, Emerich H, Paskevicius M, Buckley CE, et al. Crystalline $Al_1 - x$ Ti x phases in the hydrogen cycled $NaAlH_4 + 0.02TiCl_3$ system. Philos Mag 2012;93:1080–94.
[12] Gosalawit-Utke R, Milanese C, Javadian P, Jepsen J, Laipple D, Karmi F, et al. Nanoconfined $2LiBH_4–MgH_2–TiCl_3$ in carbon aerogel scaffold for reversible hydrogen storage. Int J Hydrogen Energy 2013;38:3275–82.
[13] Gosalawit-Utke R, Milanese C, Nielsen TK, Karimi F, Saldan I, Pranzas K, et al. Nanoconfined $2LiBH_4–MgH_2$ for reversible hydrogen storages: reaction mechanisms, kinetics and thermodynamics. Int J Hydrogen Energy 2013;38:1932–42.
[14] Javadian P, Sheppard DA, Buckley CE, Jensen TR. Hydrogen storage properties of nanoconfined $LiBH_4–Ca(BH_4)_2$. Nano Energy 2015;11:96–103.
[15] Tian HY, Buckley CE, Mulè S, Paskevicius M, Dhal BB. Preparation, microstructure and hydrogen sorption properties of nanoporous carbon aerogels under ambient drying. Nanotechnology 2008;19:475605.
[16] Hebalkar N, Arabale G, Sainkar SR, Pradhan SD, Mulla IS, Vijayamohanan K, et al. Study of correlation of structural and surface properties with electrochemical behaviour in carbon aerogels. J Mater Sci 2005;40:3777–82.
[17] Chumphongphan S, Filsø U, Paskevicius M, Sheppard DA, Jensen TR, Buckley CE. Nanoconfinement degradation in $NaAlH_4$/CMK-1. Int J Hydrogen Energy 2014;39:11103–9.
[18] Nielsen TK, Polanski M, Zasada D, Javadian P, Besenbacher F, Bystrzycki J, et al. Improved hydrogen storage kinetics of nanoconfined $NaAlH_4$ catalyzed with $TiCl_3$ nanoparticles. ACS Nano 2011;5:4056–64.
[19] Lin C, Ritter JA. Effect of synthesis pH on the structure of carbon xerogels. Carbon 1997;35:1271–8.
[20] Bogdanović B, Brand RA, Marjanovic A, Schwickardi M, Tölle J. Metal-doped sodium aluminium hydrides as potential new hydrogen storage materials. J Alloys Compd 2000;302:36–58.
[21] Jensen TR, Nielsen TK, Filinchuk Y, Jorgensen J-E, Cerenius Y, Gray EM, et al. Versatile in situ powder X-ray diffraction cells for solid-gas investigations. J Appl Crystallogr 2010;43:1456–63.
[22] Bieder H, Hoell A, Mokrani L, Zizak I. Einrichtung zur Kleinwinkelstreumessung zur Analyse der Nanostruktur an Proben mittels R€ontgenstrahlung. Patent, DE102006029449. 2007.
[23] Goerigk G, Haubold H-G, Lyon O, Simon J-P. Anomalous small-angle X-ray scattering in materials science. J Appl Crystallogr 2003;36:425–9.
[24] Stuhrmann HB. Resonance scattering in macromolecular structure research. In: Kausch HH, Zachmann HG, editors. Characterization of polymers in the solid state II: synchrotron radiation, X-ray scattering and electron microscopy. Springer Berlin Heidelberg; 1985. p. 123–63.
[25] Hoell A, Tatchev D, Haas S, Haug J, Boesecke P. On the determination of partial structure functions in small-angle scattering exemplified by $Al_{89}Ni_6La_5$ alloy. J Appl Crystallogr 2009;42:323–5.
[26] Nielsen TK, Javadian P, Polanski M, Besenbacher F, Bystrzycki J, Jensen TR. Nanoconfined $NaAlH_4$: determination of distinct prolific effects from pore size, crystallite size, and surface interactions. J Phys Chem C 2012;116:21046–51.
[27] Zheng S, Fang F, Zhou G, Chen G, Ouyang L, Zhu M, et al. Hydrogen storage properties of space-confined $NaAlH_4$ nanoparticles in ordered mesoporous silica. Chem Mater 2008;20:3954–8.
[28] Lee H-S, Lee Y-S, Suh J-Y, Kim M, Yu J-S, Cho YW. Enhanced desorption and absorption properties of eutectic $LiBH_4–Ca(BH_4)_2$ infiltrated into mesoporous carbon. J Phys Chem C 2011;115:20027–35.
[29] Paskevicius M, Tian HY, Sheppard DA, Webb CJ, Pitt MP, Gray EM, et al. Magnesium hydride formation within carbon aerogel. J Phys Chem C 2011;115:1757–66.
[30] Beaucage G. Approximations leading to a unified exponential/power-law approach to small-angle scattering. J Appl Crystallogr 1995;28:717–28.
[31] Ilavsky J, Jemian PR. Irena: tool suite for modeling and analysis of small-angle scattering. J Appl Crystallogr 2009:42.
[32] Kohls DJ, Beaucage G. Rational design of reinforced rubber. Curr Opin Solid State Mater Sci 2002;6:183–94.
[33] Bösenberg U, Vainio U, Pranzas PK, Bellosta von Colbe JM, Goerigk G, Welter E, et al. On the chemical state and distribution of Zr- and V-based additives in reactive hydride composites. Nanotechnology 2009;20:204003.
[34] Karimi F, Pranzas PK, Hoell A, Vainio U, Welter E, Raghuwanshi VS, et al. Structural analysis of calcium reactive hydride composite for solid state hydrogen storage. J Appl Crystallogr 2014;47:67–75.
[35] Pranzas PK, Bösenberg U, Karimi F, Münning M, Metz O, Minella CB, et al. Characterization of hydrogen storage materials and systems with photons and neutrons. Adv Eng Mater 2011;13:730–6.
[36] Puszkiel JA, Gennari FC, Larochette PA, Ramallo-López JM, Vainio U, Karimi F, et al. Effect of Fe additive on the hydrogenation-dehydrogenation properties of $2LiH + MgB_2$/$2LiBH_4 + MgH_2$ system. J Power Sources 2015;284:606–16.
[37] Puszkiel J, Gennari FC, Arneodo Larochette P, Troiani HE, Karimi F, Pistidda C, et al. Hydrogen storage in $Mg–LiBH_4$ composites catalyzed by FeF_3. J Power Sources 2014;267:799–811.
[38] Graetz J, Reilly JJ, Johnson J, Ignatov AY, Tyson TA. X-ray absorption study of Ti-activated sodium aluminum hydride. Appl Phys Lett 2004;85:500–2.
[39] Adelhelm P, de Jong KP, de Jongh PE. How intimate contact with nanoporous carbon benefits the reversible hydrogen desorption from NaH and $NaAlH_4$. Chem Commun 2009:6261–3.
[40] Gross KJ, Thomas GJ, Jensen CM. Catalyzed alanates for hydrogen storage. J Alloys Compd 2002;330–332:683–90.
[41] Schuth F, Bogdanovic B, Felderhoff M. Light metal hydrides and complex hydrides for hydrogen storage. Chem Commun 2004:2249–58.
[42] Zhao J, Yang L, Li F, Yu R, Jin C. Structural evolution in the graphitization process of activated carbon by high-pressure sintering. Carbon 2009;47:744–51.
[43] Brinks HW, Sulic M, Jensen CM, Hauback BC. $TiCl_3$-enhanced $NaAlH_4$: impact of excess Al and development of the Al1-yTiy phase during cycling. J Phys Chem B 2006;110:2740–5.
[44] Lohstroh W, Roth A, Hahn H, Fichtner M. Thermodynamic effects in nanoscale $NaAlH_4$. ChemPhysChem 2010;11:789–92.
[45] Gao J, Adelhelm P, Verkuijlen MHW, Rongeat C, Herrich M, van Bentum PJM, et al. Confinement of $NaAlH_4$ in nanoporous carbon: impact on H_2 release, reversibility, and thermodynamics. J Phys Chem C 2010;114:4675–82.

Please cite this article in press as: Paskevicius M, et al., Cyclic stability and structure of nanoconfined Ti-doped $NaAlH_4$, International Journal of Hydrogen Energy (2016), http://dx.doi.org/10.1016/j.ijhydene.2015.12.185